scientific reports

Check for updates

OPEN

Deep oscillatory neural network

Nurani Rajagopal Rohan[1,5], C. Vigneswaran[1,5], Sayan Ghosh[1,3], Kishore Rajendran[2], A. Gaurav[2] & V. Srinivasa Chakravarthy[1,4]✉

We propose the Deep Oscillatory Neural Network (DONN), a brain-inspired network architecture that incorporates oscillatory dynamics into learning. Unlike conventional neural networks with static internal states, DONN neurons exhibit brain-like oscillatory activity through neural Hopf oscillators operating in the complex domain. The network combines neural oscillators with traditional sigmoid and ReLU neurons, all employing complex-valued weights and activations. Input signals can be presented to oscillators in three modes: resonator, amplitude modulation, and frequency modulation. Training uses complex backpropagation to minimize the output error. We extend this approach to convolutional architectures, creating Oscillatory Convolutional Neural Networks (OCNNs). Evaluation on benchmark signal and image processing tasks demonstrates comparable or improved performance over baseline methods. Interestingly, the network exhibits emergent phenomena such as feature and temporal binding during image classification, a key characteristic of biological visual processing, and exhibit STDP (Spike Timing Dependent Plasticity) kernel when trained using Hebbain learning. These phenomena with explicit oscillatory dynamics enhance the interpretability of internal representations.

Keywords Complex-valued oscillators, Complex-valued weights, Brain-inspired networks, Sequential problems

A fundamental dichotomy persists in current large-scale models of brain function. In recent years, deep learning models, which have not been hitherto taken seriously in terms of biological plausibility, have demonstrated remarkable success in capturing sensory functions in the visual and auditory domains[1–6]. Despite their predictive power, these models do not represent the rich internal dynamics of the brain that underlie sensory processing. In contrast, non-linear oscillator networks have proven effective in accurately modeling brain dynamics observed in functional neuroimaging studies[7–9], yet they lack the capacity to learn complex input-output behavioral mappings characteristic of deep learning systems. This highlights the need for novel models that can resolve this dichotomy, and bridge the gap between the learning abilities of deep networks and the dynamic fidelity of oscillator-based approaches. In the following, we examine this dichotomy in detail and explore a potential pathway toward its resolution.

Brain oscillations represent a fundamental neurophysiological mechanism underlying cognitive functions and brain states. Research has established that oscillatory neural activity serves as the foundation for perception, memory, and higher-order cognitive processes through synchronized oscillatory networks distributed across the brain[10,11]. These neural oscillations encompass an extensive frequency spectrum, ranging from 0.05 Hz to 500 Hz[12]. This broad frequency range is organized into approximately twelve distinct frequency bands that exhibit a systematic logarithmic progression. The hierarchical organization of these frequency bands reflects both their evolutionary development and their functional specialization, with neighboring bands often associated with related cognitive and physiological states. Delta waves (0.5–4 Hz) dominate during deep sleep and recovery processes, theta oscillations (4–8 Hz) facilitate memory encoding and spatial navigation, alpha rhythms (8–12 Hz) characterize relaxed wakefulness and attention regulation, beta frequencies (13–30 Hz) support active cognition and motor control, and gamma oscillations (30–100 Hz) coordinate high-level cognitive processing and conscious awareness. This frequency-function relationship extends beyond normal physiological states, as disruptions in oscillatory patterns are consistently observed in pathological conditions including epilepsy, where abnormal synchronization patterns generate seizure activity[13], anesthesia, where altered oscillatory dynamics accompany loss of consciousness[14], and sleep disorders, where pathological oscillations impair restorative processes.

Conversely, Recurrent Neural Networks (RNNs) are traditionally used to solve sequential tasks in a variety of domains ranging from Natural Language Processing (NLP)[15,16], time-series forecasting[17,18], music generation[19],

[1]Department of Biotechnology, Indian Institute of Technology Madras, Chennai 600036, Tamil Nadu, India. [2]Department of Electrical Engineering, Indian Institute of Technology Madras, Chennai 600036, Tamil Nadu, India. [3]Department of Computer Science and Engineering, SRM University-AP, Amaravati 522502, Andhra Pradesh, India. [4]Center for Complex Systems and Dynamics, Indian Institute of Technology Madras, Chennai 600036, Tamil Nadu, India. [5]These authors contributed equally: Nurani Rajagopal Rohan and C. Vigneswaran. ✉email: schakra@ee.iitm.ac.in

video analysis[20], etc. Popular variants of vanilla RNNs like Long Short-Term Memory units (LSTMs)[21], Gated Recurrent Unit (GRUs)[22], flip-flop[23] neural networks are widely used for different kinds of sequential problems and achieve state-of-the-art performance. These sequential networks can operate in different modes namely, many-to-one (eg. sentiment analysis)[24], one-to-many (eg. handwriting generation)[25] and, many-to-many (eg. machine translation)[26]. Recurrent units with convolutional operations on the gating variables are used to capture spatio-temporal features in video processing tasks[27]. Some recent studies have constructed complex network-based embeddings and neural manifolds to classify EEG data and improve interpretability[28,29]. In recent years, deep neural networks (DNN) have been shown to match human performance in pattern recognition in visual and auditory domains[1,2]. Studies that demonstrated a similarity in human performance with that of DNNs, have further shown that even human error pattern with respect shape variation[30], viewpoint variation[3,4] and object class[5,6] also matched with DNN error patterns. However, this broad match in error patterns did not carry over into errors committed on classification of individual images[31]. Similarly in the auditory domain, studies based on DNNs have shown a close performance match in music and speech recognition[32–34]. Despite these remarkable successes in achieving human-like behavioral performance, the aforementioned deep learning models are unable to capture the oscillatory activity of brain dynamics.

Considering the fundamental importance of oscillations in brain function, any comprehensive large-scale model of neural dynamics must necessarily accommodate oscillatory brain activity and reflect the empirically established significance of various frequency bands. Neural mass models[35] have emerged as a computational framework for describing brain dynamics at mesoscopic and macroscopic levels. In contrast to detailed biophysical models that simulate individual neurons, neural mass models represent the collective behavior of neural populations as their fundamental computational unit. Popular low dimensional models have been utilized to describe the oscillatory dynamics. The Hopf oscillator, which generates stable limit-cycle oscillations via supercritical bifurcations and can entrain to inputs; the Wilson-Cowan model[36], which describes excitatory–inhibitory interactions and produces gamma-band rhythms; the FitzHugh–Nagumo oscillator[37], a reduced excitability model that reproduces spike-generation and synchronization; and the Kuramoto model[38,39], which characterizes phase synchronization across large oscillator networks. Theoretical analysis of networks of excitatory and inhibitory neurons have revealed rich resonance due to various phenomena, particularly stochastic resonance[40,41]. These oscillatory network models have demonstrated remarkable success in reproducing brain dynamics as measured through functional neuroimaging techniques including functional magnetic resonance imaging (fMRI), magnetoencephalography (MEG), and high-density electroencephalography (EEG)[42–47]. However, a critical limitation emerges when the functional capabilities of these oscillatory networks are examined. Although they excel at capturing the dynamic signatures of brain activity, they fundamentally lack the input-output learning capacity that characterizes biological neural systems. This represents a profound constraint on their applicability as general models of brain function. Current implementations of oscillatory networks, when applied to behavioral modeling, remain predominantly restricted to intrinsically rhythmic or periodic behaviors. Examples include central pattern generator models for locomotor movements in quadrupedal gaits[48], oscillatory control of rhythmic hand movements during repetitive tasks[49], and coordination of swimming motions in aquatic locomotion[50].

Research has highlighted that these observed oscillatory responses in cortical systems are not only a reflection of the fixed network property, but a task-dependent phenomenon, emerging dynamically through a causal chain, from the interaction between network connectivity and external drive. This observation has important modeling implications; to capture such emergent coordination faithfully, computational frameworks cannot completely rely on static coupling schemes alone. Instead, oscillatory network models must, in addition, be endowed with the capacity to exhibit input-contingent oscillatory phenomena, allowing their collective dynamics to flexibly adapt to task demands. Incorporating this principle is essential, as oscillations serve not only as products of intrinsic neuronal and network dynamics but also as mechanisms for context-dependent, transient binding or segregation of neuronal populations and represent a fundamental and salient condition for modeling the full spectrum of brain function.

From the above considerations, there is a clear need to develop deep neural networks in which the hidden layers are constituted of oscillatory neuron models. The networks must be capable of learning input/output behaviour like any deep neural network. In this paper we address this challenge and present a general class of trainable deep oscillatory neural networks. The outline of the paper is as follows. In Sect. 2, we apply this network to a class of benchmark problems that involve sequential processing. We describe the results obtained and compare them with results from other non-oscillatory deep neural networks. Section 3 describes the development of the model and the equations that govern dynamics and learning. Section 4 discusses the results and outlines how the present class of networks can be developed further to improve their biological plausibility.

Results

The DONN was implemented in Python 3.9.11 and TensorFlow 2.10.1, and run on an x86 CPU and NVIDIA GPU under Windows 11. Further implementation details are provided in the Supplementary Information. We demonstrate the capability of DONN in a variety of sequential processing tasks (some additional tasks have been included in the Supplementary Information).

Temporal sequence processing and classification

We describe the ability of DONN to extract Fourier-type features to be able to perform time series classification. We construct a synthetic dataset for temporal classification in which each datapoint consists of five independent signals.

Initial frequency range of oscillators	[0.1-20 Hz]
Architecture	Linear (20),Hopf (20), $\tanh$ (20), output (2)
Input type to oscillators	$I(t)$
Frequency of oscillators	Not trained

Table 1. Network architecture for Classification.

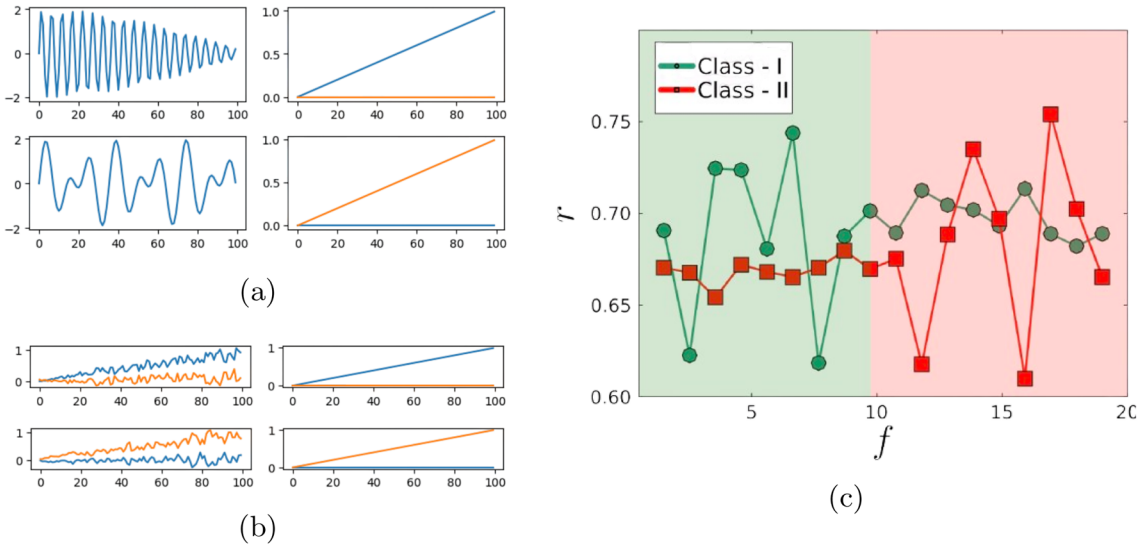

Figure 1. (**a**) Training Samples from the dataset are shown on the left with the corresponding labels on the right. (**b**) Some sample model predictions are shown on the left and are compared with the corresponding labels to indicate correct classification. (**c**) A comparison of the internal dynamics of Hopf oscillator activations in response to two samples from separate datasets. Stimulating the network with a signal from class-1, the amplitudes of the oscillators with intrinsic frequency in the range 0.1–10 Hz show differential amplitudes when compared to the oscillators with higher intrinsic frequency, whereas Class-2 inputs activate oscillators in the 10–20 Hz band.

$$I(t) = \sum_{i=1}^{5} A_i \sin(2\pi f_i t + \phi_i) \tag{1}$$

The amplitudes A_i are sampled uniformly from [-3, 3], and the phases are drawn uniformly from $[0, 2\pi]$. The dataset is divided into two classes based on the frequency content of the signals. In Class 1, the frequencies of all five signals lie within the low-frequency band, $f \in [0, 10]$ Hz, whereas in Class 2, the frequencies are sampled from the higher band, $f \in [10, 20]$ Hz. This controlled setup enables clear discrimination based on frequency features, while preserving diversity through randomization in amplitude and phase across data points.

The details of the network architecture are described in Table 1 which achieves an accuracy of 99% on this binary classification task. We analyze the hidden layer's oscillatory activity to understand how the network encodes and differentiates input signals. By stimulating the network with signals from the dataset, we examine the resulting amplitudes of the oscillators in the hidden (oscillatory) layer to infer class-specific internal representations. Upon presentation of dataset signals, the amplitude responses of oscillators reveal class-specific tuning: signals from Class-1 lead to heightened activity in the 0.1–10 Hz frequency band, while signals from Class-2 primarily engage the 10–20 Hz oscillators, see Fig. 1.

Amplitude demodulation

In order to transmit a signal over a distance without being affected by external interference or noise and without experiencing degradation, it must undergo a modulation process. The inverse process of retrieving the message is demodulation. We show that our network is able to perform this operation. The mathematical expression for amplitude modulation is given as follows,

$$\mathcal{M}(t) = (1 + m(t)) \sin(\omega_c t) \tag{2}$$

where $m(t)$ is the message signal, ω_c is the carrier wave frequency and M(t) is the modulated signal. For this task the message signal, $m(t) = \sum_{i=1}^{5} \sin(2\pi f_i t)$, $f_i \in \mathcal{U}(1, 5)$ Hz. Carrier frequency, $\omega_c = 8$ Hz is kept fixed.

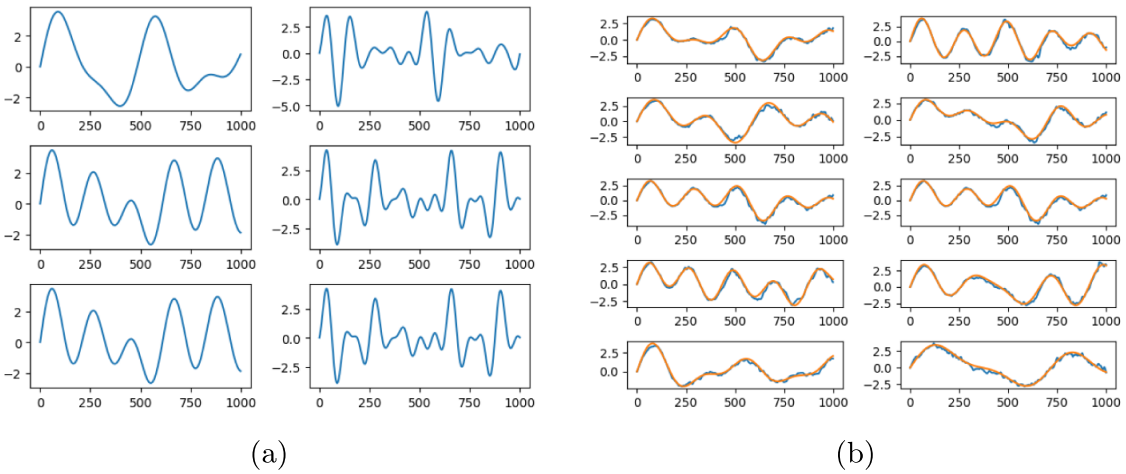

Figure 2. (**a**) (Left) The message signals composed of up to five frequency components i.e., $m(t) = \sum_{i=1}^{5} \sin(2\pi f_i t)$, $f_i \in \mathcal{U}(1, 5)$ Hz. (Right) the corresponding modulated signals described by Eq. (2). (**b**) The performance of our model in demodulating the signal. The desired demodulated signals are in *orange* and the model predictions are in *blue*.

Input frequency range	Carrier: 8 Hz, message signal: [1-5 Hz]
Initial frequency range of oscillators	[0.1-12 Hz]
Architecture	ReLU (40),Hopf (40), ReLU (40),Hopf (40), tanh (40), output (1)
Input type to oscillators	$I(t)$
Frequency of oscillators	Not trained

Table 2. Network architecture for Amplitude Demodulation.

Some sample message signals and the corresponding modulated signals are given in Fig. 2a. The size details of the network architecture are described in Table 2. The oscillators are initialised with frequency in the range 0.1 Hz to 12 Hz. The input to the oscillator is given as $I(t)$. The network is able to demodulate the message signal accurately (Fig. 2b). The validation MSE loss is 0.02 ($\mathrm{p} < 0.05$, $\mathrm{n} = 10$).

Learning mathematical operators

In this task the network is trained to perform indefinite integration and differentiation on synthetically generated sinusoidal signals : **Data**, the data is composed of signals with multiple frequency components and arbitrary initial phase offset and amplitude. If $I(t) = \sum_i a_i \sin(\omega_i t + \phi_i)$ is the input signal, the output signal, then for the integration task, $O(t)$ is given by,

$$O(t) = \sum_i -\frac{a_i}{\omega_i} \cos(\omega_i t + \phi_i) \tag{3}$$

and for the differentiation is given by,

$$O(t) = \sum_i a_i \omega_i \cos(\omega_i t + \phi_i) \tag{4}$$

where a_i, ϕ_i, ω_i are the amplitude, phase offsets and the angular frequencies sampled from $\mathcal{N}(0, 1)$, $\mathcal{N}(0, \pi)$ and $\mathcal{U}(1, 5)$ respectively.

The size details of the network architecture for the task is described in Table 3. The network successfully performs the integration operation and the differentiation operation on the dataset, see Fig. 3. For integration, Data-1 the validation MSE loss is 0.08 ($\mathrm{p} < 0.05$, $\mathrm{n} = 10$), and the MSE loss for Differentiation is 0.1, ($\mathrm{p} < 0.05$, $\mathrm{n} = 10$).

Sentiment analysis

Movie review sentiment analysis typically involves a two-class classification problem (positive/negative). The IMDB large movie review dataset[51] serves as a common benchmark for sentiment analysis tasks, with a predefined maximum review length of 500 words. The training data is split into training and validation in a 7 :

	Data 1
Input frequency range	[0.1-5 Hz]
Initial frequency range of oscillators	[1-10 Hz]
Architecture	ReLU (20),Hopf (20), ReLU (20), Hopf (20), $\tanh$ (20), output (1)
Input type to oscillators	$I(t)$
Frequency of oscillators	Not trained

Table 3. Network architecture for Learning Mathematical Operations.

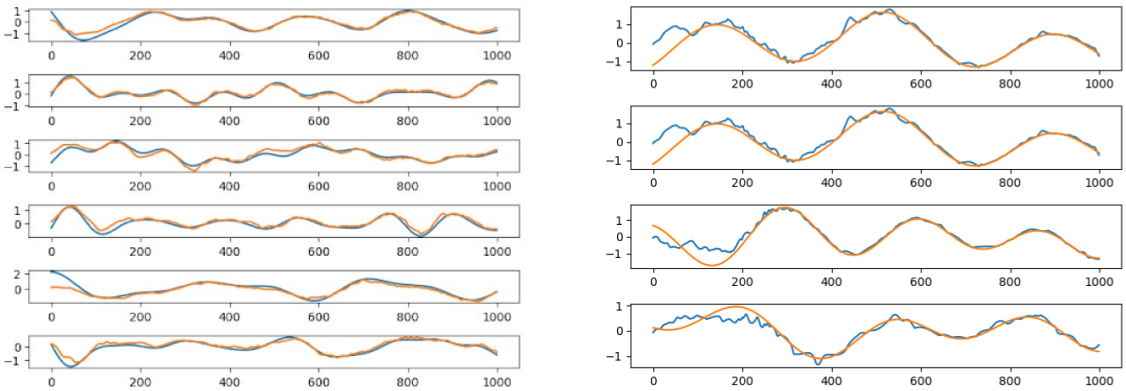

(a) (b)

Figure 3. (**a**) The network is able to learn the Integration operation, some sample figures are shown where the model predictions shown in orange are compared with desired signals in blue. (**b**) The network is able to learn the Differentiation operation, some sample figures are shown, where the desired outputs (orange) and model predicted outputs (blue) are shown.

Model	Validation accuracy	Architecture
Bidirectional LSTM [23]	85.19%	Embedding layer (100), 2 x Bidirectional flip-flops (100), $\tanh$ (20),output (2)
Bidirectional flipflop [23]	85.07%	Embedding layer (100), 2 x Bidirectional flip-flops (100), $\tanh$ (20),output (2)
DONN	85.2 %	Embedding layer (100), Hopf (100),ReLU (100), Hopf (100),ReLU (100), $\tanh$ (20), output (2) Initial frequency range of oscillators: [1-15 Hz], Input type to oscillators: $I(t)$, Frequency of oscillators: trained

Table 4. Sentiment analysis.

3 ratio. The selection of this task aims to demonstrate the proficiency of the Deep Oscillator Neural Network in sequence classification.

The words are encoded and passed to the embedding layer followed by the DONN. The embedding dimension is 100 with a vocabulary length of 35,000. The input to the oscillator layer is presented as $I(t)$. The total trainable parameters is 26,798. The optimiser used is the ADAM optimiser with learning rate = 0.001, and the objective function used is mean squared error. The model achieves a performance of 85.2% ($p < 0.05$, $n = 10$) accuracy on testing data. The network architecture and comparison with other models are described in Table 4

Spatiotemporal sequence processing and classification

Action recognition : UCF 11

To showcase the sequence processing capacity of OCNN network in spatiotemporal domain, we validate the network using UCF11 YouTube Action dataset[52]. UCF11 is a standard 3-channel RGB video classification dataset with different viewpoints, backgrounds and camera motions. The dataset consists of 11 action classes, and number of frames for all the videos is set to 50, with each frame resized to 48×48 from the original 224×224, on account of limited computational capability. Dataset is divided into training and validation with 1290 and 305 samples respectively. The network used for the task consists of two pairs of convolutional-oscillators layers, followed by flattening and dense layers. The architecture details of the network used for the task is mentioned in Table 5. Time step of the oscillators is set to 0.02 seconds with the number of time steps equal to the number of frames in a video sample. Adam (learning rate: 0.0001) and MSE are used as optimizer and loss function respectively for training.

Model	Validation accuracy	Architecture
Convolutional LSTM [23]	95.42%	2 x ConvLSTM (3x3,40), Conv3D (3x3x3, 1), flatten, softmax (2)
Convolutional flip-flops[23]	99.75%	2 x ConvLSTM (3x3,40), Conv3D (3x3x3, 1), flatten, softmax (2)
OCNN	98.64%	2 x OCNN (3x3,40), flatten, output (2) Initial frequency range: [1-15 Hz], Input type to oscillator: $I(t)$, Frequency of oscillators: trained

Table 5. Action recognition.

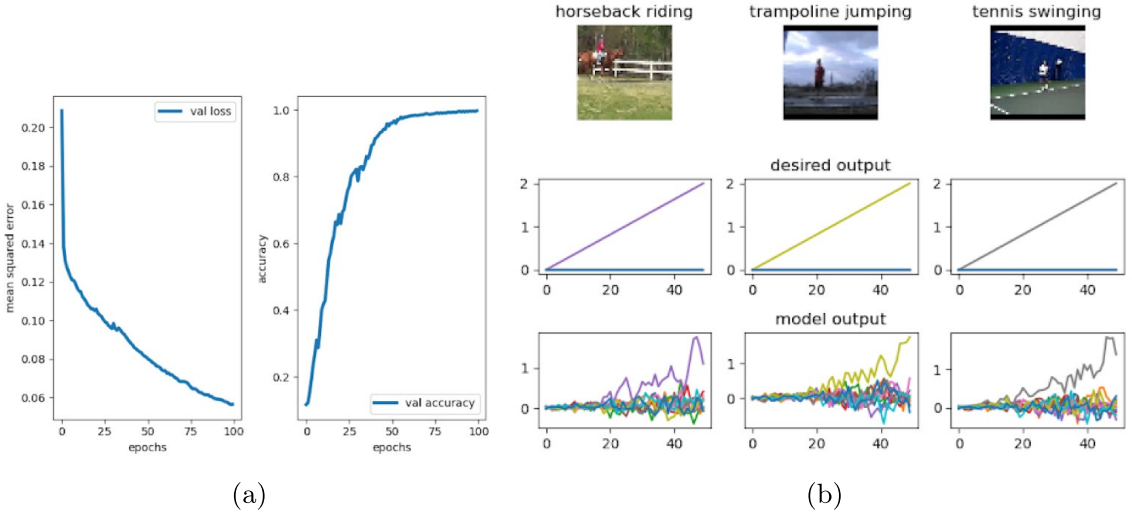

Figure 4. (**a**) Accuracy and loss plots on validation data for UCF11 dataset. (**b**) Sample frames of the input and their corresponding classes mentioned above, and the desired and the model predicted ramp output. Only one class ramps up linearly whereas all other classes remain zero throughout.

Figure 4a shows the accuracy and loss curves on validation data, Fig. 4b and the desired output and output from the model. The validation MSE loss and accuracy of the model is 0.0564 and 99.75% ($p < 0.05$, $n = 10$) respectively.

Case study 1: temporal binding analysis with respect to color and orientation selection in ConvOsc network
Several works in the literature draw parallels between artificial convolutional neural networks (CNNs) and the visual pathways of the brain[1,6,53]. Although CNNs are well known for compressing spatial features, the visual system of the brain processes both spatial and temporal features simultaneously. Different visual properties of the input stimulus (color, form, direction of motion etc) are processed in different visual cortical areas. This presents an interesting problem. If a subject is looking at a yellow disc moving up, and a red circle moving right, if the the color ('yellow' and 'red'), form ('square' and 'circle') and motion ('up' and 'right), how does the brain associate or bind different properties to different objects? An elegant solution offered to this problem is known as temporal binding. Accordingly, neurons whose firing activity represents different properties of the same object fire in synchrony. Thus it has been suggested that brain is using the temporal dimension to solve the binding problem. There is also neurobiological evidence to temporal binding from mammalian visual systems[54]. Temporal binding has also been demonstrated in spiking neural network models[4]. In this case study, we demonstrate that networks incorporating ConvOsc layers not only generalize effectively for classification tasks but also exhibit hidden-layer activations that capture temporal feature-binding characteristics.

The task is to perform classification of videos from four classes: green horizontal moving bar, green vertical moving bar, red horizontal moving bar and red vertical moving bar. Parameters such as speed, width, and initial position of the bar are varied in generating input videos. The predicted winning class is chosen by the ramp approach. The model architecture and the hidden layer dimensions are mentioned in the Fig. 5. For this study, oscillators only from the second ConvOsc layer of the model is used. The following are the steps taken for temporal binding analysis.

1. Selection of color and orientation selective oscillators.
2. Group oscillators by union of color and orientation for the particular input class.
3. Calculate synchrony within the oscillators of the group and the remaining oscillators.

We now describe the algorithm that we used for the analysis of temporal binding:

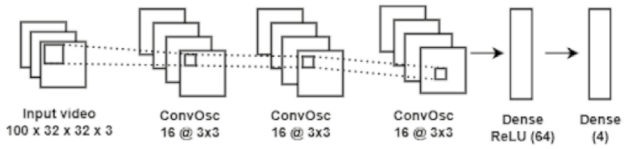

Figure 5. Model architecture and its hidden layer dimensions for temporal binding analysis study. All oscillators in the network are initialized in the range, 1–10 Hz.

1. Let input video be of class (A, X) with color A and orientation X (where set colors (red, green): {A, B}, orientation (vertical, horizontal): {X, Y}, respectively).
2. Calculate the amplitude of the oscillators' responses $|z_i|$.
3. Let *AX* be the set of oscillators whose amplitude $|z_i|$ exceeds a defined threshold for an input video belonging to class (*A*, *X*). Similarly, compute the sets *AY*, *BX*, and *BY* as the oscillators whose amplitude $|z_i|$ exceeds the threshold for input videos belonging to classes (*A*, *Y*), (*B*, *X*), and (*B*, *Y*), respectively.
4. Define the sets of color- and orientation-selective oscillators as follows:

- **Color-selective oscillators:**

$$\hat{A} = (AX \cup AY) - (BX \cup BY)$$
$$\hat{B} = (BX \cup BY) - (AX \cup AY)$$

- **Orientation-selective oscillators:**

$$\hat{X} = (AX \cup BX) - (AY \cup BY)$$
$$\hat{Y} = (AY \cup BY) - (AX \cup BX)$$

$\cup$ and $-$ denote set union and difference operations respectively. These sets ensure that oscillators are uniquely selective to either a specific color or orientation, excluding those that respond to both.

5. The **group oscillators corresponding to each input class** are given by:

$$\hat{A}\hat{X} = \text{Group oscillators obtained from } \hat{A} \cup \hat{X}$$
$$\hat{A}\hat{Y} = \text{Group oscillators obtained from } \hat{A} \cup \hat{Y}$$
$$\hat{B}\hat{X} = \text{Group oscillators obtained from } \hat{B} \cup \hat{X}$$
$$\hat{B}\hat{Y} = \text{Group oscillators obtained from } \hat{B} \cup \hat{Y}$$

6. To quantify the synchrony among oscillators, we compute synchrony *S* for the following sets:

- **Group oscillators:** $\hat{A}\hat{X}, \hat{A}\hat{Y}, \hat{B}\hat{X}, \hat{B}\hat{Y}$.
- **Residuary oscillators:** $U\text{-}\hat{A}\hat{X}, U\text{-}\hat{A}\hat{Y}, U\text{-}\hat{B}\hat{X}, U\text{-}\hat{B}\hat{Y}$ (*U* is the set of all oscillators in the second ConvOsc layer).

The synchrony *S* within a set of *N* oscillators over a time period *T* is computed using the formula:

$$S = \frac{1}{T}\sum_{t=1}^{T}\left|\frac{1}{N}\sum_{i=1}^{N}\frac{z_i(t)}{|z_i(t)|}\right| \tag{5}$$

The above steps are repeated $n = 20$ times, and the synchrony plot for the group and residuary oscillators in the second ConvOsc layer for different input classes is shown in Fig. 6. The number of oscillators in the sets $\hat{A}$, $\hat{X}$, $\hat{B}$, and $\hat{Y}$ are summarized in Table 6. The results indicate that higher synchrony is achieved in the group oscillators compared to residuary oscillators across all 20 trials. Thus, the DONN network can show temporal binding characteristics.

Case study 2: emergence of STDP (spike timing-dependent plasticity) kernel when a pair of coupled Hopf oscillators are trained using Hebb's rule

The nature of oscillatory dynamics allows for more robust temporal relationships that are less sensitive to noise and timing jitter compared to the precise spike timing requirements of STDP-based systems. Interestingly, the emergence of potentiation and the spike-time-dependent plasticity (STDP) kernel can be captured in a conjugately coupled pair of Hopf oscillators with complex weight *W*. The oscillators are driven by pulsed inputs, with one receiving the pulse after a delay of τ relative to the other. As a result of this interaction, the weights

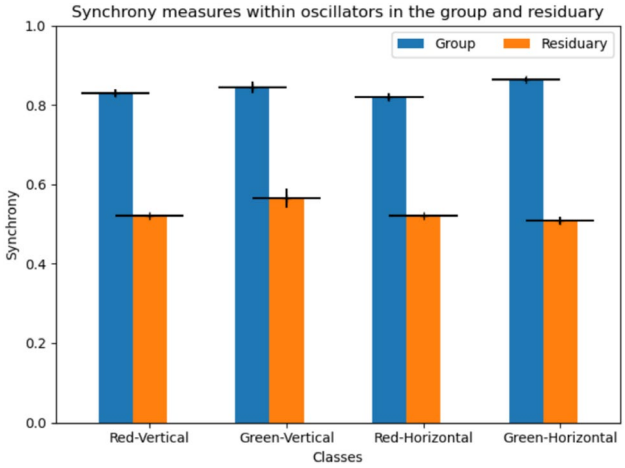

Figure 6. Synchrony values for group and residuary oscillators in the second ConvOsc layer for different input classes. Group oscillators ($\hat{A}\hat{X}, \hat{A}\hat{Y}, \hat{B}\hat{X}, \hat{B}\hat{Y}$) and residuary oscillators ($U - \hat{A}\hat{X}, U - \hat{A}\hat{Y}, U - \hat{B}\hat{X}, U - \hat{B}\hat{Y}$) are obtained from the corresponding input classes (Red-Vertical, Green-Vertical, Red-Horizontal, Green-Horizontal). Higher synchrony measures within the oscillators of Group than those of Residuary indicates temporal binding characteristics.

Set	Number of Oscillators
$\hat{A}$	545
$\hat{X}$	435
$\hat{B}$	38
$\hat{Y}$	48

Table 6. Number of oscillators in the color-selective sets: $\hat{A}$, B, and orientation-selective sets: $\hat{X}$, $\hat{Y}$.

evolve such that the real component captures potentiation, while the imaginary component encodes the STDP kernel. The dynamical equations are given by

$$\dot{z}_1 = (\mu + i\omega_1)z_1 - |z_1|^2 z_1 + W z_2 + p(t), \tag{6}$$

$$\dot{z}_2 = (\mu + i\omega_2)z_2 - |z_2|^2 z_2 + \overline{W} z_1 + p(t+\tau), \tag{7}$$

$$\dot{W} = -W + \eta\, z_1\, \overline{z_2}. \tag{8}$$

The weight updates are plotted as a function of the delay τ, see Fig. 7. However, this method is not employed in our analysis for solving any of the tasks.

Hardware benchmarking

In this section, the computational efficiency of DONN is compared with LSTM in terms of number of trainable parameters and execution time (GPU and CPU). Execution time is time elapsed in forward propagation of input data through the network. Two networks comprising of single layer of LSTM and DONN (no. of units=50) seperately are used for comparison. Figure 8 shows the comparison results for both networks. It can be inferred that DONN is more computationally efficient than LSTM, except for the execution time in GPU where Tensorflow's LSTM module is CUDA compiled and leveraged CuDNN kernels for faster execution. The better performance of DONN in hardware benchmarking when compared to LSTM can be due to the usage of LSTM's three gates (trainable parameter sets) and two outputs (cell and hidden) for sequence processing, whereas in DONN only complex-valued parameters are to trained. Despite having a significantly smaller number of trainable parameters and execution time, DONN can outperform LSTM in many of the sequence processing tasks. Please refer to the Supplementary Information for further results.

Methods

The oscillatory neuron model we use in our networks is the Hopf oscillator. It is a harmonic oscillator with a stable limit cycle. The canonical Hopf oscillator is described by the following complex valued differential equation,

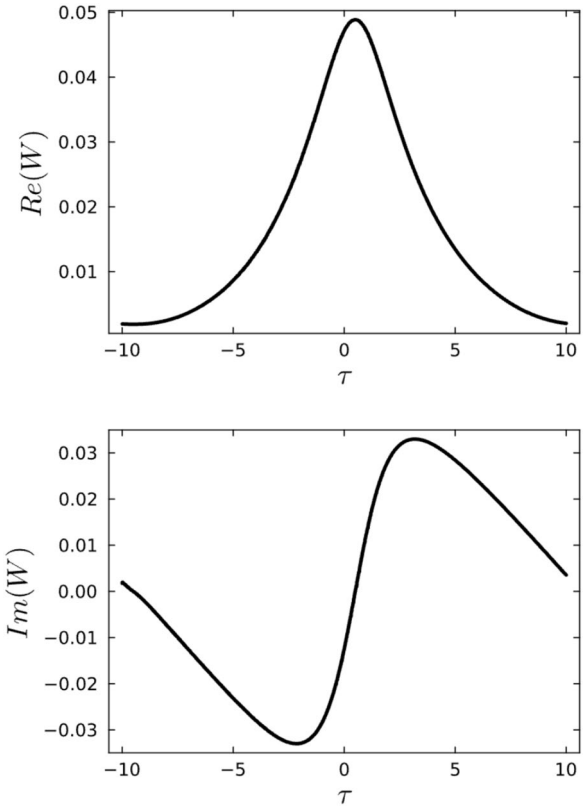

Figure 7. The weights kernels for one period of oscillations is shown. We see that the $Re(W)$ encoded the potentiation whereas the $Im(W)$ encodes the STDP kernel.

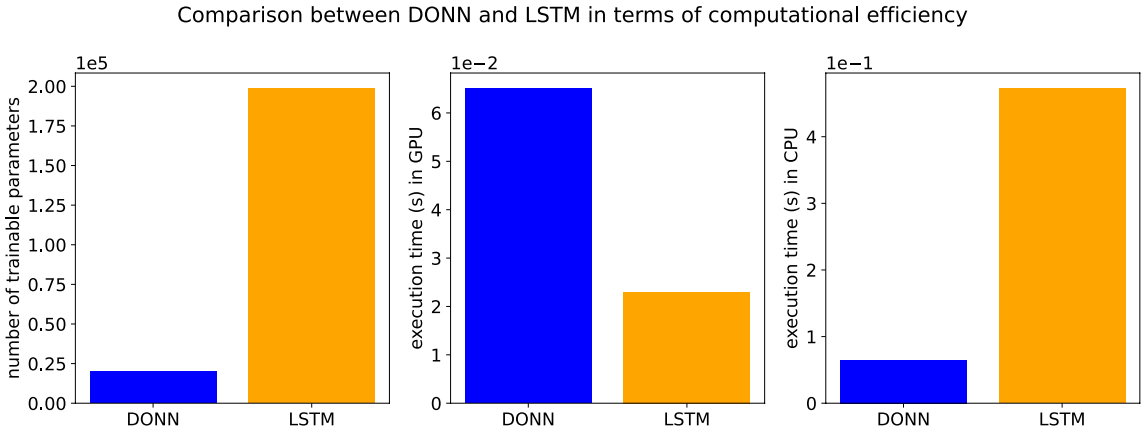

Figure 8. Comparison between DONN and LSTM with respect to number of trainable model parameters and execution time (GPU & CPU).

$$\dot{z} = z\left(\mu + \iota\omega + \beta_1|z|^2 + \frac{\epsilon\beta_2|z|^4}{1-\epsilon|z|^2}\right) + I(t). \tag{9}$$

where ω is the natural angular frequency of the Hopf oscillator, μ governs Hopf bifurcation, and $I(t)$ is the external input to the oscillator. If $z = x + \iota y$, then the polar coordinate form is received by introducing the variables,

$$\theta = \arctan\frac{y}{x}, \quad r = (x^2 + y^2)^{1/2}. \tag{10}$$

The polar coordinate representation is more explicate for our analysis and is given as follows,

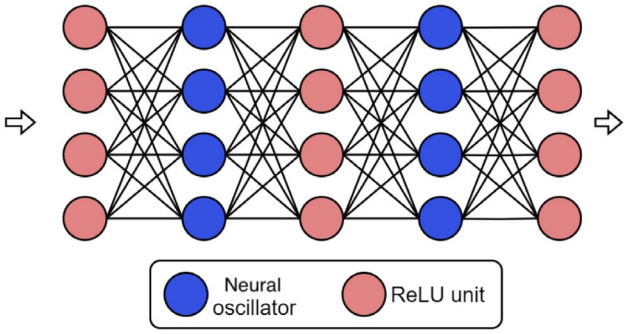

Figure 9. The Oscillatory Neural Network is generally composed of alternating static and oscillatory layers.

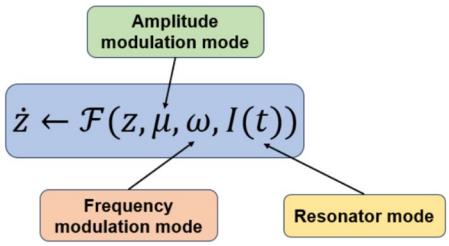

Figure 10. Mechanisms through which the input, $z_{in}(t)$ can be presented to the Oscillator unit.

$$\begin{aligned} \dot{r} &= \mu r + \beta r^3 + \frac{\epsilon \beta_2 r^5}{1 - \epsilon r^2} + A(t)\ \cos\ \psi \\ \dot{\psi} &= \Omega - \frac{A(t)}{r}\ \sin\ \psi \end{aligned} \tag{11}$$

where $r(t)$ is the instantaneous amplitude of oscillation and $\psi(t)$ is its instantaneous angular position. The external input is given by, $I(t) = A(t)e^{i\phi(t)}$ where $A(t)$ is the instantaneous amplitude and $\phi(t)$ the instantaneous phase angle. Further, we have introduced the transformation, $\psi = \theta - \phi(t)$, and $\Omega = \omega - \frac{\mathrm{d}\phi}{dt}$ is the difference between the angular frequencies of the oscillator and the external input. In the absence of an external input, the oscillator exhibits four distinct dynamical behaviors characterized by the parameters (μ, β_1, β_2) – critical Hopf regime $(\mu = 0, \beta_1 < 0, \beta_2 = 0)$, supercritical Hopf regime $(\mu > 0, \beta_1 < 0, \beta_2 = 0)$, double limit cycle regime $(\mu < 0, \beta_1 > 0, \beta_2 < 0)$. We restrict our attention to the critical or supercritical regime $(\beta_2 = 0)$; for a more detailed analysis on the others see[55]. The equations Eq. (9) then transform to,

$$\dot{z} = z\left(\mu + \iota\omega + \beta|z|^2\right) + I(t). \tag{12}$$

$$\begin{aligned} \dot{r} &= \mu r + \beta r^3 + A(t)\ \cos\ \psi \\ \dot{\psi} &= \Omega - \frac{A(t)}{r}\ \sin\ \psi \end{aligned} \tag{13}$$

In the absence of an external signal, the system undergoes Hopf bifurcation at $\mu = 0$. For fixed β, if $\mu \geq 0$, the system has an unstable fixed point at $r^* = 0$ and a stable fixed point as $r^* = \sqrt{\frac{\mu}{\beta}}$, and such that the system exhibits self-sustained oscillations with amplitude $\sqrt{\frac{\mu}{\beta}}$. When $\mu < 0$, $r^* = 0$ is the only stable fixed point of the system; in which case there is no oscillations. The proposed oscillator neural network model consists of successive layers of static, dense or convolutional layers with nonlinear activation and dynamic Hopf oscillator layers. A general oscillator neural network is depicted in Fig. 9. There are three modes in which an input, $z_{in}(t)$, can be presented to the oscillator layer for forward propagation; either as external input $I(t)$, referred to as resonator mode, or as input to the amplitude $\mu(t)$, commonly referred as amplitude modulation mode, or as input to the frequency $\omega(t)$, referred to as frequency modulation mode, Fig. 10). The method of forward pass for the three modes of input to a single oscillator unit is described below,

1. **Resonator mode (Input presented as $I(t)$):** In the presence of an external complex periodic driving of angular frequency ω_0, $z_{in}(t) = I(t) = I_0 e^{\iota\omega_0 t}$, Eq. (13) for the case of supercritical Hopf bifurcation transforms to,

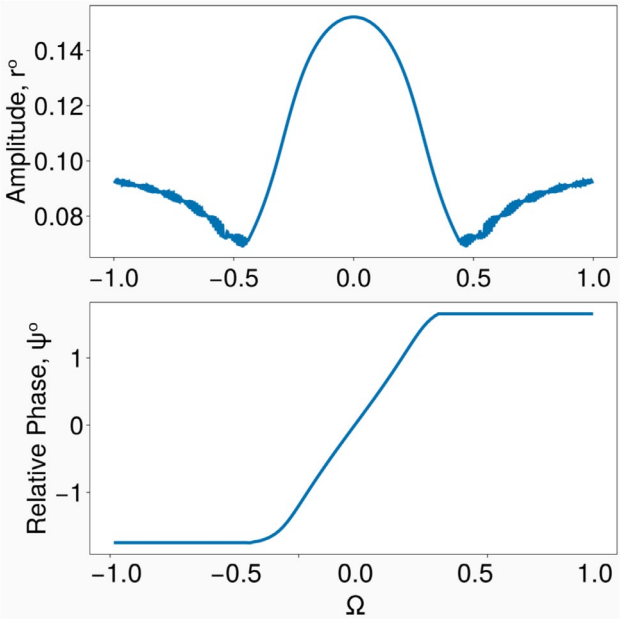

Figure 11. Driven behaviour of a supercritical Hopf oscillator under strong forcing. Steady-state amplitude and relative phase as a function of frequency difference describe the resonance characteristics. The parameters used are $(\mu = 1, \beta_1 = -100, \beta_2 = 0, I_0 = 0.2)$.

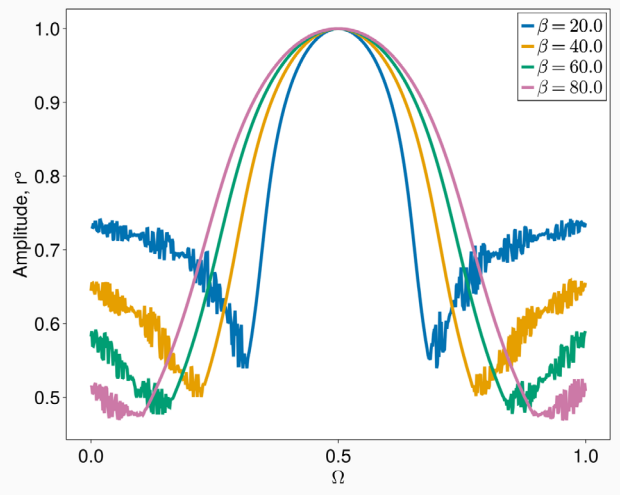

Figure 12. The bandwidth of the resonant curve increases with increasing β. The curves are normalized to 1 to accentuate the effect on the bandwidth.

$$\begin{aligned} \dot{r} &= \mu r + \beta r^3 + \kappa_I I_0 \cos \psi \\ \dot{\psi} &= \Omega - \kappa_I \frac{I_0}{r} \sin \psi \end{aligned} \tag{14}$$

where $\psi = \theta - \omega_0 t$ is the relative phase and $\Omega = \omega - \omega_0$ is the difference between the angular frequencies of the oscillator and the external input, respectively. The steady state solution of the system can be analyzed by fixed point analysis. The fixed points of the system is obtained by solving $\dot{r}, \dot{\psi} = 0$ simultaneously. In the presence of strong forcing $(I_0 \approx 10^{-1})$, the behavior of a supercritical Hopf oscillator is given in Fig. 11. The oscillator shows resonance in a small range of frequencies around its natural frequency. The oscillator activation is then in a frequency locked state with the input signal i.e., the frequency of the oscillator activation is equal to the frequency of the input signal. Furthermore, within the smaller range of frequency, the oscillator activation is in a phase locked state to the input signal, see Fig. 11. Beyond this regime, the system undergoes phase slip. As β increases, the bandwidth of the resonant curve increases, see Fig. 12.

We note that the resonance described in Fig. 11 is only valid for when the input is of the particular form, $I(t) = I_0 e^{\iota\omega_0 t}$. In the case $I(t)$ is composed of $n-$complex sinusoids, $I(t) = \sum_{i=1}^{n} I_i e^{\iota\omega_i t}$, the resonant tuning curves depend on I_i and ω_i. The dynamical equations are transformed to

$$\begin{aligned} \dot{r} &= \mu r + \beta r^3 + \kappa_I \sum_{i=1}^{N} I_i \cos(\theta - \omega_i t) \\ \dot{\theta} &= \omega - \frac{\kappa_I}{r} \sum_{i=1}^{N} I_i \sin(\theta - \omega_i t) \end{aligned} \tag{15}$$

where ω_i is the angular frequency of the input signal is kept constant, and ω is the intrinsic frequency of the oscillator is allowed to vary. For ω closer to ω_k, we introduce the variables $\psi = \theta - \omega_k t$ and average the equation for them, we get Eq. (14). Therefore within a small neighborhood of ω_k, we get a similar resonant curve as in Fig. 11. This aligns with numerical simulations as described in Figs. 13 and 14.

2. **Amplitude Modulation (Input presented as $\mu(t)$):** In this case, with $z_{in}(t)$ as input to the r equation of the oscillator, the dynamical equations are given by,

$$\mu(t) = (\mu_0 + \kappa_\mu \Re(z_{in}(t))) \tag{16}$$

$$\begin{aligned} \dot{r_i} &= \mu(t) r_i + \beta r_i^3 \\ \dot{\theta_i} &= \omega_i \end{aligned} \tag{17}$$

where, $\Re$ denotes the real part of the complex number. Since the amplitude of the oscillator is a positive quantity, one must ensure that, $\kappa_\mu \min(\Re(z_{in})) + \mu_0 > 0$ where $\min(\Re(z_{in}))$ is the minimum value of $\Re(z_{in}(t))$.

3. **Frequency Modulation (Input presented as $\omega(t)$):** In this case, $z_{in}(t)$ is given as input to the θ equation of the oscillator. In this case, the input modulates the effective oscillator frequency as follows:

$$\begin{aligned} \dot{r_i} &= \mu r_i + \beta r_i^3 \\ \dot{\theta_i} &= \omega_i + \kappa_\omega \Re(z_i(t)) \end{aligned} \tag{18}$$

In the latter two modes of the input, the Hopf oscillation activation gets modulated by the input oscillations, hence the name. In this paper, we only use the first two modes of input presentation to the neural oscillator. The above differential equations are solved from $t = 0 \ldots T$ using Forward Euler method with fixed time step relevant to the dataset. Suppose the solution to either of the above systems is given $\{r, \theta\}$, then the output is given by,

$$\mathfrak{Z}_d(t) = (r\cos\theta + \iota\, r \sin\theta) \tag{19}$$

As depicted in Fig. 9, the complex activation, Eq. (19), of the oscillator layer feeds into a static layer. The complex nonlinear activation, is then applied as follows,

$$\mathfrak{Z}_s(t) = \mathfrak{f}(\Re(\mathfrak{Z}_d(t))) + \iota \mathfrak{f}(\Im(\mathfrak{Z}_d(t))) \tag{20}$$

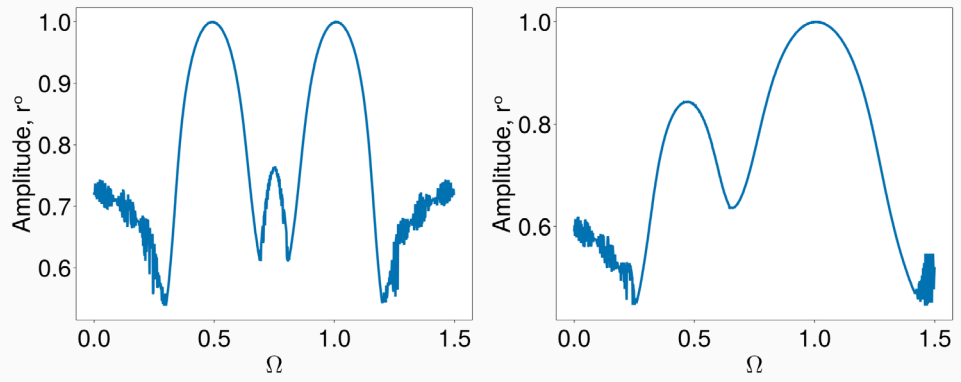

Figure 13. We show the resonant tuning curve for $n = 2$ with equal (Left) and unequal (Right) strength of forcing with $I_1/I_2 = 0.5$. The other parameters are $\mu = 1, \beta = 20$.

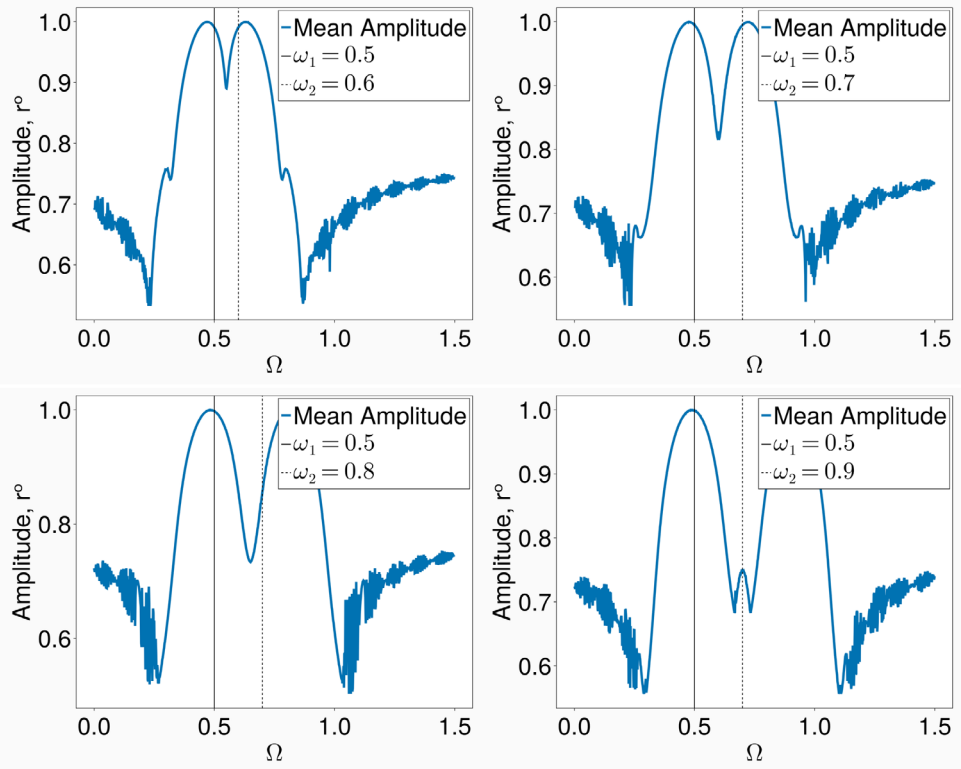

Figure 14. Starting from top-left and moving clockwise, the resonant tuning curves are presented for incremental ω_2.

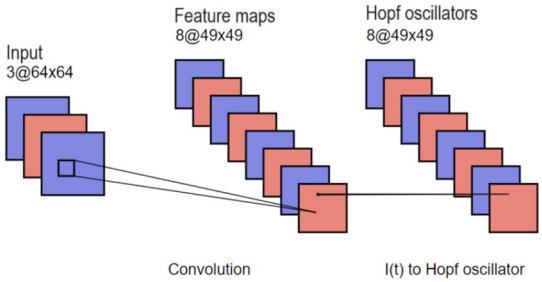

Figure 15. Convolutional Oscillatory block: feature maps obtained after convolutional operation on input image at time t is given as input $I(t)$ in one-to-one fashion to oscillatory block of dimension equal to that of feature maps to obtain spatio-temporal feature maps.

point wise in time. Where $\Re, \Im$ denote the real part and imaginary part of the complex numbers. The complex nonlinear activation can be ReLU, $\tanh$, or sigmoid function.

All the functions mentioned above are piecewise continuously differentiable. We use automatic differentiating feature (autograd) of TensorFlow library to calculate the gradients for backpropogation to update network weights.

Oscillatory convolutional neural network (OCNN)

In our proposed OCNN model, due to the presence of oscillatory elements, neurons of higher layers possess spatio-temporal responses. Arrangement of oscillators are identical to the input feature maps to maintain the spatial information. The intrinsic frequencies of the oscillators are sampled from a uniform random distribution of appropriate range. The frequency distribution is passed through a Gaussian blur of kernel size 3x3 across the 2D arrangements of oscillators in each channel. Hierarchical arrangements of such pairs of convolution and oscillators enable learning and detection of features at different levels of complexities in spatiotemporal scale, see Fig. 15.

Classification using oscillatory neural network

Due to the dynamic nature of the DONN model, the output of the network is always a time series. If the network is tasked with a classification problem, the labels have to be defined differently. In order to have an equivalent classification score for oscillator activation, we use the ramp approach to decide the predicted class. Ramp-like classifications are often used in biological models as they closely replicate the race-based threshold criterion to select the winner neurons[56]. For each time step, all classes' (corresponding neurons in the last layer) desired predictions are zero, except for the desired class where the desired value rises linearly. The predicted class is decided by selecting the neuron which has the maximum average across time steps.

Discussions and concluding remarks

We present a broad class of trainable deep oscillatory neural networks that can be trained on a variety of classification problems. We also presented an oscillatory analog of CNNs called as OCNNs that can be used to classify videos. We argue that the proposed class of DONNs are able to overcome some longstanding limitations of the existing oscillatory network models in computational neuroscience and in artificial neural networks.

In computational neuroscience modelling, oscillatory neural networks have been used in several subdomains of neuroscience. For instance, rhythmic movements underlying locomotion are thought to be driven by special neural circuits known as Central Pattern Generators (CPGs), capable of generating oscillatory dynamics[57–60]. Thus oscillatory networks have been used to model the rhythmic movements of locomotion in bipeds or quadrupeds[48,61], or swimming movements[50], and rhythmic movements of a robotic hand[49]. Some early models of locomotion used fixed connections, with bio-inspired architecture, but later models like those from Ijspeert and colleagues[62] are trainable models. However, this latter class of models are purely generative models i.e. they are not I/O models and generate an output without any input.

Additionally, although our modeling strategy relies on the hypothesis that information is encoded in the ensemble activity of neurons, Spiking Neural Networks (SNNs) have long been regarded as the prototypical framework for brain-inspired computing, owing to their biologically plausible learning mechanisms. Unsupervised approaches like spike-time-dependent plasticity (STDP) depend on the specification of an integration window to infer correlated versus uncorrelated activity, with synaptic weights subsequently updated according to Hebbian learning. The time window integration definition is nebulous which can result in inaccurate inferences. The DONN approach offers several mechanistic advantages over discrete spike-timing methods. The complex-valued representation in DONN enables the encoding of both amplitude and phase information simultaneously, providing a richer representational space than binary spike events. The continuous phase/amplitude variables of Hopf oscillators admit direct, low-dimensional measures (phase synchrony, amplitude envelopes, spectral content) that are straightforward to visualize and interpret, improving transparency relative to spike-raster statistics, and permits widely applicable analytic approximations (statistical mechanics tools – phase reduction through an order parameter) that can help explain why particular frequency and coupling choices yield binding.

Recent years have witnessed rapid advances in spiking neural networks (SNNs), motivated by their event-driven computation, energy efficiency, and biological plausibility. For instance, Stanojevic et al.[63] demonstrated high-performance deep SNNs with ultra-low activity budgets, achieving competitive accuracy with only $\sim$0.3 spikes per neuron. Shen et al.[64] proposed an efficient continual learning framework based on sparse selective activation, enabling SNNs to balance stability and plasticity in dynamic environments. Structural innovations have also been introduced: Shi et al.[65] developed the *SpikingResformer*, which bridges ResNet and Vision Transformer architectures in the spiking domain, while Xu et al.[66] integrated a spiking convolutional block attention module to enhance recurrent architectures for adaptive history reserving. More recently, Shen et al.[67] introduced temporal attention-guided adaptive fusion to address imbalanced multi-modal learning in SNNs.

The proposed Deep Oscillatory Neural Network framework complements these efforts (brain-inspired computing) by adopting this fundamentally different representational paradigm. Rather than encoding information through discrete spike events, DONN leverages the continuous dynamics and the nonlinear interactions among Hopf oscillators. Further, we have shown that the STDP kernel emerges in a pair of coupled Hopf oscillators whose weights are trained using the Hebb's rule.

When it comes to applications of oscillatory networks in sensory processing, an important class of models is dedicated to feature binding. The problem of feature binding addresses the question of how the brain binds the different sensory characteristics like color, form, texture to construct the presentation of a single object. It has been proposed that such binding can be achieved temporally by synchronizing the oscillations underlying various sensory characteristics, a mechanism known as temporal feature binding[68]. A number of oscillatory neural networks have been proposed to describe temporal feature binding in perception[69], multisensory integration[70], working memory[71]. Oscillatory neural networks are naturally suited to modelling auditory processing of music, thanks to the intrinsic rhythmicity of the signal, and have therefore been applied to music perception[34,55]. The aforementioned class of oscillatory neural networks either have fixed connections or are trained by unsupervised learning in cases where learning occurs. Whereas, in the current work, the proposed network is trainable using supervised-backpropagation and can be generalized to multiple paradigms.

In the temporal binding analysis case study, we have showed that how color-selective and orientation-selective oscillators are synchronized temporally to encode the features from the input video. Emergence of synchrony between desired oscillatory groups to learn the task shows the proposed class of models can be used to explain feature binding mechanisms. The current work only showed the feature binding between oscillatory groups from the same layer and it can extended to show the emergence of hierarchical features representations at different layers. Such a network will be a good model of the entire visual system pathway and can capture complex phenomena such as how neurons in different levels synchronize to solve aperture problem[72]. Although stimulus-induced synchronization is often associated with increased firing rates of responding neurons, our modeling

approach is primarily based on reflecting the mesoscopic view of brains activity, where ensemble synchrony can also occur in the absence of firing-rate changes at the single-neuron level. In such cases, conventional single-unit methods are insufficient, as spikes from a single neuron do not reveal the cooperative performance of the network. By contrast, the oscillatory framework of DONN explicitly encodes ensemble synchrony in continuous phase relationships, making such cooperative dynamics directly observable and quantifiable. Moreover, viewing the activity of the non oscillatory layers as rate codes, the mean field activity of the neural Hopf layers representing the spatial-temporal statistical properties can serve as a useful reference to which activity of single static neurons can be related.

Then there is a rich body of modelling literature that applies oscillatory neural networks to model brain dynamics at large scale. These models are calibrated by various types of functional readouts of the brain like eg fMRI[42,73], Electroencephalogram (EEG)[46,74–76], or Magnetoencephalogram (MEG)[77]. In addition to describing the normal brain, this class of models have been applied to model brain dynamics in conditions of brain disorders including Alzheimers[78], Stroke[79] , Parkinson's disease[80] etc. In this class of models, typically, the network connections are not a result of learning but are obtained from the empirical structural connectivity of the brain. However, a recent modelled study had proposed use of complex-valued connections in which the magnitudes are obtained from structural connectivity while the phase is learnt by a modified form of Hebbian learning[43].

Apart from the aforementioned biologically oriented examples, there have been a range of artificial engineering applications of oscillatory neural networks. An important class refers to associative memory models. Earliest associative memory models are based on fixed point dynamics[81,82], which have low biological plausibility and are artificial since memories in the brain are necessarily composed of neural oscillations[83,84]. This motivation had inspired a range of oscillatory associative memories[85,86]. In the earliest models of oscillatory associative memories all the oscillators had the same intrinsic frequency. Deficiencies in storage capacity shown by oscillatory associative memories that operate at a single frequency are overcome by generalizations that involve an addition of harmonics to the dynamics, apart from the fundamental frequency[87–89]. Note that in this entire class of oscillatory neural networks are trained by unsupervised learning, more specifically a variation of Hebbian learning. Other artificial applications of oscillatory neural networks include image segmentation, auditory scene segmentation and object detection. Note that the class of oscillatory networks described in this para involve an unsupervised learning rules like Hebbian learning or its variations and therefore cannot learn I/O behavior.

Recent years saw a surge of interest in the area of hardware implementations of oscillatory neural networks[90]. In the 1950s, von Neumann had proposed that oscillators can be used as logic gates and digital information can be stored in the form of phase differences[91,92]. Current oscillatory neural hardware implementations encompass associative memories[93], image and audio segmentation[94,95] and memristor models of locomotor rhythms[61]. Thus, the hardware implementations of the above oscillatory networks also cannot learn I/O behavior. These implementations of neural networks, often called neuromorphic systems, often use spiking neuron networks[96]. Interestingly, the boundary between oscillator-based compute (OBC) circuits and spiking neural networks (SNNs) is somewhat diffuse: OBC circuit designs share many functional and architectural features with spiking neurons. Although spiking neural networks often rely on oscillatory mechanisms to generate temporal signals, they generally do not exploit the nonlinear interactions between oscillators that can give rise to rich dynamical phenomena such as resonance, entrainment, and synchronization[90]. In contrast, the proposed Deep Oscillatory Neural Network (DONN) explicitly harnesses these nonlinear interactions, using phase, amplitude, and frequency dynamics as computational primitives to achieve biologically grounded and interpretable representations, at low power. Further, there are possible implementation of oscillators where energy is recycled among oscillators instead of being discharged, which could be a suitable candidate for OBC. There is a possibility of both these fields to merge for computationally and power efficient hardware implementations.

The current implementation of DONN is restricted to input-driven feedforward connections, however the activities of cortical neuronal ensembles at the mesoscopic scale is both stimuli-driven and self-organized. Such neuronal organization will be more biologically-plausible and better representatives. We have restricted our current implementation to a supervised learning framework. However, many interesting biological phenomena are observed in Reinforcement learning framework; such high vs low gamma in spatial learning observed in striatum[97], self organized oscillations emerging during memory consolidation in sleep[98], and prominent synchronized beta frequency in Subthalamic Nucleus of the Basal ganglia observed in Bradykinesia[99]. Biological systems excel at solving the binding problem, the segmenting cluttered scenes and the analysis of complex time series (e.g., spoken language). As future work, we aim to extend our networks to describe such complex neurological phenomena.

The broad class of DONNs described in this paper, which to our knowledge is perhaps the first demonstration of a deep oscillatory neural network with multiple frequencies, trainable in an I/O fashion, is expected to be a valuable addition to oscillatory neural network literature.

Data availability

Data is provided within the manuscript or supplementary information files.

Code availability

Source code can be accessed in the Google Drive link.

Received: 29 July 2025; Accepted: 15 October 2025
Published online: 20 November 2025

References

1. Kell, A. J., Yamins, D. L., Shook, E. N., Norman-Haignere, S. V. & McDermott, J. H. A task-optimized neural network replicates human auditory behavior, predicts brain responses, and reveals a cortical processing hierarchy. *Neuron* **98**, 630-644.e16 (2018).
2. Huang, Y. et al. Brain-inspired robust vision using convolutional neural networks with feedback (2019). https://openreview.net/forum?id=rylU4mtUIS.
3. Wardle, S. G., Taubert, J., Teichmann, L. & Baker, C. I. Rapid and dynamic processing of face pareidolia in the human brain. *Nat. Commun.* **11**, 4518 (2020).
4. Wardle, S. G. & Baker, C. I. Recent advances in understanding object recognition in the human brain: deep neural networks, temporal dynamics, and context. *F1000Research***9** (2020).
5. Geirhos, R. et al. Imagenet-trained cnns are biased towards texture; increasing shape bias improves accuracy and robustness (2022). arXiv:1811.12231.
6. Cichy, R. M., Khosla, A., Pantazis, D., Torralba, A. & Oliva, A. Comparison of deep neural networks to spatio-temporal cortical dynamics of human visual object recognition reveals hierarchical correspondence. *Sci. Rep.* **6**, 27755 (2016).
7. Bick, C., Goodfellow, M., Laing, C. R. & Martens, E. A. Understanding the dynamics of biological and neural oscillator networks through exact mean-field reductions: a review. *J. Math. Neurosci.* **10**, 9 (2020).
8. Chinichian, N. et al. Modeling brain network flexibility in networks of coupled oscillators: a feasibility study. *Sci. Rep.* **14**, 5713 (2024).
9. Laing, C. R. Phase oscillator network models of brain dynamics. *Comput. Models Brain Behav.* 505–517 (2017).
10. Kahana, M. J. The cognitive correlates of human brain oscillations. *J. Neurosci.* **26**, 1669–1672 (2006).
11. Dang-Vu, T. & Courtemanche, R. *Neuronal Oscillations of Wakefulness and Sleep: Windows on Spontaneous Activity of the Brain* (Springer, New York, 2020).
12. Buzsáki, G. & Draguhn, A. Neuronal oscillations in cortical networks. *Science* **304**, 1926–1929 (2004).
13. Blanco, J. A. et al. Data mining neocortical high-frequency oscillations in epilepsy and controls. *Brain* **134**, 2948–2959 (2011).
14. Akeju, O. & Brown, E. N. Neural oscillations demonstrate that general anesthesia and sedative states are neurophysiologically distinct from sleep. *Curr. Opin. Neurobiol.* **44**, 178–185 (2017).
15. Xiao, J. & Zhou, Z. Research progress of rnn language model (2020).
16. Otter, D. W., Medina, J. R. & Kalita, J. K. A survey of the usages of deep learning for natural language processing. *IEEE Trans. Neural Netw. Learn. Syst.* **32**, 604–624 (2020).
17. Hewamalage, H., Bergmeir, C. & Bandara, K. Recurrent neural networks for time series forecasting: Current status and future directions. *Int. J. Forecast.* **37**, 388–427 (2021).
18. Lim, B. & Zohren, S. Time-series forecasting with deep learning: a survey. *Phil. Trans. R. Soc. A* **379**, 20200209 (2021).
19. Briot, J.-P. & Pachet, F. Deep learning for music generation: challenges and directions. *Neural Comput. Appl.* **32**, 981–993 (2020).
20. Xu, Z., Hu, J. & Deng, W. Recurrent convolutional neural network for video classification (2016).
21. Hochreiter, S. & Schmidhuber, J. Long short-term memory. *Neural Comput.* **9**, 1735–1780. https://doi.org/10.1162/neco.1997.9.8.1735 (1997).
22. Chung, J., Gulcehre, C., Cho, K. & Bengio, Y. Empirical evaluation of gated recurrent neural networks on sequence modeling (2014). arXiv:1412.3555.
23. Kumari, S., Chandrasekaran, V. & Chakravarthy, V. The flip-flop neuron: a memory efficient alternative for solving challenging sequence processing and decision-making problems. *Neural Comput. Appl.* (2023).
24. Gopalakrishnan, K. & Salem, F. M. Sentiment analysis using simplified long short-term memory recurrent neural networks (2020). arXiv:2005.03993.
25. Graves, A. Generating sequences with recurrent neural networks (2014). arXiv:1308.0850.
26. Tan, Z. et al. Neural machine translation: A review of methods, resources, and tools. *AI Open* **1**, 5–21 (2020).
27. Shi, X. et al. Convolutional lstm network: A machine learning approach for precipitation nowcasting (2015). arXiv:1506.04214.
28. Yu, H., Lei, X., Song, Z., Liu, C. & Wang, J. Supervised network-based fuzzy learning of eeg signals for alzheimer's disease identification. *IEEE Trans. Fuzzy Syst.* **28**, 60–71 (2019).
29. Yu, H., Zeng, F., Liu, D., Wang, J. & Liu, J. Neural manifold decoder for acupuncture stimulations with representation learning: An acupuncture-brain interface. *IEEE J. Biomed. Health Inf.* (2025).
30. Atabay, H. A. Deep residual learning for tomato plant leaf disease identification. *J. Theor. Appl. Inf. Technol.* **95** (2017).
31. Rajalingam, B., Priya, R. & Scholar, R. Review of multimodality medical image fusion using combined transform techniques for clinical application. *Int. J. Sci. Res. Comp Sci. App.* **7**, 1–8 (2018).
32. Large, E. W. et al. Dynamic models for musical rhythm perception and coordination. *Front. Comput. Neurosci.* **17** (2023).
33. Hinton, G. et al. Deep neural networks for acoustic modeling in speech recognition: The shared views of four research groups. *IEEE Signal Process. Mag.* **29**, 82–97 (2012).
34. Chou, S.-Y., Cheng, K.-H., Jang, J.-S. R. & Yang, Y.-H. Learning to match transient sound events using attentional similarity for few-shot sound recognition (2019).
35. Pinotsis, D., Robinson, P., beim Graben, P. & Friston, K. Neural masses and fields: modeling the dynamics of brain activity (2014).
36. Cowan, W. M., Gottlieb, D., Hendrickson, A. E., Price, J. & Woolsey, T. The autoradiographic demonstration of axonal connections in the central nervous system. *Brain Res.* **37**, 21–51 (1972).
37. Nagumo, J., Arimoto, S. & Yoshizawa, S. An active pulse transmission line simulating nerve axon. *Proc. IRE* **50**, 2061–2070 (1962).
38. Cumin, D. & Unsworth, C. Generalising the kuramoto model for the study of neuronal synchronisation in the brain. *Phys. D* **226**, 181–196 (2007).
39. Breakspear, M., Heitmann, S. & Daffertshofer, A. Generative models of cortical oscillations: neurobiological implications of the kuramoto model. *Front. Hum. Neurosci.* **4**, 190 (2010).
40. Yu, H. et al. Multiple stochastic resonances and oscillation transitions in cortical networks with time delay. *IEEE Trans. Fuzzy Syst.* **28**, 39–46 (2020).
41. Yu, H. et al. Firing rate oscillation and stochastic resonance in cortical networks with electrical–chemical synapses and time delay. *IEEE Trans. Fuzzy Syst.* **28**, 5–13 (2020).
42. Jirsa, V. & Woodman, M. M. *& Domide, L* (Simulation environment for large-scale brain networks, The virtual brain (tvb), 2022).
43. Bandyopadhyay, A., Ghosh, S., Biswas, D. & et al. A phenomenological model of whole brain dynamics using a network of neural oscillators with power-coupling. *Sci. Rep.***13**, 16935 (2023).
44. Cabral, J., Hugues, E., Sporns, O. & Deco, G. Role of local network oscillations in resting-state functional connectivity. *Neuroimage* **57**, 130–139 (2011).
45. Bey, P. et al. Lesion aware automated processing pipeline for multimodal neuroimaging stroke data and the virtual brain (tvb). *bioRxiv* 2023–08 (2023).
46. Sanz Leon, P. et al. The virtual brain: a simulator of primate brain network dynamics. *Front. Neuroinform.* **7**, 10 (2013).
47. Deco, G., Jirsa, V., Sporns, O. & Kötter, R. Key role of coupling, delay, and noise in resting brain fluctuations. *Proc. Natl. Acad. Sci.* **106**, 10302–10307 (2009).
48. Dutra, M., de Pina Filho, A. & Romano, V. Modeling of a bipedal locomotor using coupled nonlinear oscillators of van der pol. *Biol. Cybern.* **88**, 286–292 (2003).
49. Lakatos, D., Petit, F. & Albu-Schäffer, A. Nonlinear oscillations for cyclic movements in human and robotic arms. *IEEE Trans. Rob.* **30**, 865–879 (2014).

50. Cao, Y., Bi, S., Cai, Y. & Zhang, L. Applying coupled nonlinear oscillators to imitate swimming modes of cow-nosed rays (2013).
51. Maas, A. L. et al. Learning word vectors for sentiment analysis (2011).
52. Liu, J., Luo, J. & Shah, M. Recognizing realistic actions from videos "in the wild" (2009).
53. Lindsey, J., Ocko, S. A., Ganguli, S. & Deny, S. A unified theory of early visual representations from retina to cortex through anatomically constrained deep cnns. arXiv:1901.00945 (2019).
54. Engel, A. K. & Singer, W. Temporal binding and the neural correlates of sensory awareness. *Trends Cogn. Sci.* **5**, 16–25 (2001).
55. Kim, J. C. & Large, E. Signal processing in periodically forced gradient frequency neural networks. *Front. Comput. Neurosci.* **9** (2015).
56. Kumari, S. & Chakravarthy, V. S. Biologically inspired image classifier based on saccadic eye movement design for convolutional neural networks. *Neurocomputing* **513**, 294–317 (2022).
57. Alexander, R. M. The gaits of bipedal and quadrupedal animals. *Int. J. Robot. Res.* **3**, 49–59 (1984).
58. Maufroy, C., Kimura, H. & Takase, K. Towards a general neural controller for quadrupedal locomotion. *Neural Netw.* **21**, 642–653 (2008).
59. Grillner, S. Neural networks for vertebrate locomotion. *Sci. Am.* **274**, 64–69 (1996).
60. Ivashko, D. G., Prilutsky, B. I., Markin, S. N., Chapin, J. K. & Rybak, I. A. Modeling the spinal cord neural circuitry controlling cat hindlimb movement during locomotion. *Neurocomputing* **52–54**, 331–338 (2003).
61. Bonagiri, A. & Biswas, D. *& Chakravarthy, S* (Modeling and analysis. IEEE Transactions on Neural Networks and Learning Systems, Coupled memristor oscillators for neuromorphic locomotion control, 2022).
62. Ijspeert, A. J. Central pattern generators for locomotion control in animals and robots: A review. *Neural Netw.* **21**, 642–653 (2008).
63. Stanojevic, A. et al. High-performance deep spiking neural networks with 0.3 spikes per neuron. *Nat. Commun.* **15**, 6793 (2024).
64. Shen, J., Ni, W., Xu, Q. & Tang, H. *Efficient spiking neural networks with sparse selective activation for continual learning* https://doi.org/10.1609/aaai.v38i1.27817 (2024).
65. Shi, X., Hao, Z. & Yu, Z. Spikingresformer: Bridging resnet and vision transformer in spiking neural networks. arXiv:2403.14302 (2024).
66. Xu, Q. et al. Enhancing adaptive history reserving by spiking convolutional block attention module in recurrent neural networks (2024). arXiv:2401.03719.
67. Shen, J. et al. Spiking neural networks with temporal attention-guided adaptive fusion for imbalanced multi-modal learning (2025). arXiv:2505.14535.
68. Gray, C., König, P., Engel, A. & Singer, W. Oscillatory responses in cat visual cortex exhibit inter-columnar synchronization which reflects global stimulus properties. *Nature* **338**, 334–337 (1989).
69. Isokawa, T., Nishimura, H., Kamiura, N. & Matsui, N. Perceptual binding by coupled oscillatory neural network (2005).
70. Rao, A. R. An oscillatory neural network model that demonstrates the benefits of multisensory learning. *Cogn. Neurodyn.* **12**, 481–499 (2018).
71. Pina, J. E., Bodner, M. & Ermentrout, B. Oscillations in working memory and neural binding: A mechanism for multiple memories and their interactions. *PLoS Comput. Biol.* **14**, e1006517 (2018).
72. Heeger, D. J. Optical flow using spatiotemporal filters. *Int. J. Comput. Vis.* **1**, 279–302 (1988).
73. Sip, V. et al. Characterization of regional differences in resting-state fmri with a data-driven network model of brain dynamics. *Sci. Adv.* **9**, eabq7547 (2023).
74. Ghosh, S., Biswas, D., Vijayan, S. & Chakravarthy, V. S. Modeling whole brain electroencephalogram (eeg) in a spatially organized oscillatory neural network. *bioRxiv* **2023.07.16.549247** (2023).
75. Al-Hossenat, A., Wen, P. & Li, Y. Large-scale brain network model and multi-band electroencephalogram rhythm simulations. *Int. J. Biomed. Eng. Technol.* **38**, 395–409 (2022).
76. Schirner, M., McIntosh, A. R., Jirsa, V., Deco, G. & Ritter, P. Inferring multi-scale neural mechanisms with brain network modelling. *elife* **7**, e28927 (2018).
77. Schäfer, C. B., Morgan, B. R., Ye, A. X., Taylor, M. J. & Doesburg, S. M. Oscillations, networks, and their development: Meg connectivity changes with age. *Hum. Brain Mapp.* **35**, 5249–5261 (2014).
78. Yang, L. et al. Alzheimer's disease: Insights from large-scale brain dynamics models. *Brain Sci.* **13**, 1133 (2023).
79. Idesis, S. et al. Inferring the dynamical effects of stroke lesions through whole-brain modeling. *NeuroImage: Clin.* **36**, 103233 (2022).
80. Kim, J. et al. Abnormal intrinsic brain functional network dynamics in parkinson's disease. *Brain* **140**, 2955–2967 (2017).
81. Hopfield, J. J. Neural networks and physical systems with emergent collective computational abilities. *Proc. Natl. Acad. Sci.* **79**, 2554–2558 (1982).
82. Hopfield, J. J. Neurons with graded response have collective computational properties like those of two-state neurons. *Proc. Natl. Acad. Sci.* **81**, 3088–3092 (1984).
83. Freeman, W. J. *Mass Action in the Nervous System* (Academic Press, 1975).
84. Freeman, W. J. & Barrie, J. M. Analysis of spatial patterns of phase in neocortical gamma eegs in rabbit. *J. Neurophysiol.* **84**, 1266–1278 (2000).
85. Imai, Y. & Taniguchi, T. Associative memory by virtual oscillator network based on single spin-torque oscillator. *Sci. Rep.* **13**, 15809 (2023).
86. Chakravarthy, S. & Ghosh, J. A complex-valued associative memory for storing patterns as oscillatory states. *Biol. Cybern.* **75**, 229–238 (1996).
87. Aonishi, T. Phase transitions of an oscillator neural network with a standard hebb learning rule. *Phys. Rev. E* **58**, 4865–4871 (1998).
88. Nishikawa, T., Hoppensteadt, F. C. & Lai, Y.-C. Oscillatory associative memory network with perfect retrieval. *Phys. D* **197**, 134–148 (2004).
89. Follmann, R., Macau, E. E. N., Rosa, E. & Piqueira, J. R. C. Phase oscillatory network and visual pattern recognition. *IEEE Trans. Neural Netw. Learn. Syst.* **26**, 1539–1544 (2015).
90. Csaba, G. & Porod, W. Noise immunity of oscillatory computing devices. *IEEE J. Explor. Solid State Comput. Dev. Circ.* **6**, 164–169 (2020).
91. Von Neumann, J., Churchland, P. M. & Von Neumann, K. *The Computer and the Brain* (Yale University Press, 2000).
92. Wigington, R. L. A new concept in computing. *Proc. IRE* **47**, 516–523 (1959).
93. Nikonov, D. E., et al. Coupled-oscillator associative memory array operation for pattern recognition. *IEEE J. Explor. Solid-State Comput. Devices Circ.* **1**, 85–93 (2015).
94. Rudner, T., Porod, W. & Csaba, G. Design of oscillatory neural networks by machine learning. *Front. Neurosci.* **18** (2024).
95. Abernot, M. et al. Digital implementation of oscillatory neural network for image recognition applications. *Front. Neurosci.* **15** (2021).
96. Rathi, N. et al. Exploring neuromorphic computing based on spiking neural networks: Algorithms to hardware. *ACM Comput. Surv.* **55**, 243 (2023).
97. Van Der Meer, M. A. & Redish, A. D. Low and high gamma oscillations in rat ventral striatum have distinct relationships to behavior, reward, and spiking activity on a learned spatial decision task. *Front. Integr. Neurosci.* **3**, 544 (2009).
98. Buzsáki, G. *Rhythms of the Brain* (Oxford university press, 2006).
99. Wilkins, K. B. et al. Bradykinesia and its progression are related to interhemispheric beta coherence. *Ann. Neurol.* **93**, 1029–1039 (2023).

Acknowledgements
The first author would like to acknowledge the financial assistance by Council for Scientific and Industrial Research (CSIR).

Author contributions
N.R.R, V.C. - Conceptualization, Methodology, Software, Validation, Writing - Original Draft, S.G, K.R., G.A. - Software V.S.C. - Conceptualization, Writing - Original Draft, Writing - Review & Editing, Supervision, Validation.

Funding
N.R.R. would like to acknowledge the financial assistance by Council for Scientific and Industrial Research (CSIR).

Declarations

Competing interests
The authors declare no competing interests.

Additional information
Supplementary Information The online version contains supplementary material available at https://doi.org/10.1038/s41598-025-24837-4.

Correspondence and requests for materials should be addressed to V.S.C.

Reprints and permissions information is available at www.nature.com/reprints.

Publisher's note Springer Nature remains neutral with regard to jurisdictional claims in published maps and institutional affiliations.